Journal of Sound and Vibration (2000) **230**(4), 791–808
doi:10.1006/jsvi.1999.2653, available online at http://www.idealibrary.com on IDEAL®

USE OF NON-DEGENERACY IN NOMINALLY AXISYMMETRIC STRUCTURES FOR FAULT DETECTION WITH APPLICATION TO CYLINDRICAL GEOMETRIES

T. J. ROYSTON AND T. SPOHNHOLTZ

The University of Illinois at Chicago, Chicago, IL 60607, *U.S.A.*

AND

W. A. ELLINGSON

Argonne National Laboratory, Argonne, IL 60439, *U.S.A.*

(*Received* 1 *February* 1999, *and in final form* 13 *September* 1999)

A novel technique is proposed for the detection of localized flaws in otherwise axisymmetric structures. The technique is based on the split-mode phenomena that occurs when the degenerate vibratory modes of the axisymmetric structure become non-degenerate due to the flaw with altered mode shapes and shifted natural frequencies. A basic theoretical motivation is offered and computational and experimental studies on cylindrical structures are reported that verify the premises of the proposed methodology and provide an assessment of its specificity and sensitivity under confounding conditions, such as out-of-roundness.

1. INTRODUCTION

Finite elastic solids of nominally axisymmetric geometry, such as circular plates, rings, and cylinders are found in many critical applications, in the form of pipes, shafts, heat exchanger tubes, turbine blisks (bladed disks), combustion liners, saw blades, disk brakes, etc. For some of these components, where vibratory modes involve substantial flexural motion that varies with the angular location, the particular nature of their vibratory behavior can be highly dependent on relatively minor, localized imperfections (sources of non-axisymmetry) in their geometry. Perfectly axisymmetric continuous structures possess an infinite number of pairs of degenerate modes of vibration with identical natural frequencies and mode shapes that are identical except for a shift in angular orientation. For example, modes of a flat circular plate with one or more nodal diameters are degenerate. There are two modes with "n" nodal diameters that have identical natural frequencies and have mode shapes that are identical except for a shift in the angular orientation of the nodal diameters. While there must be a relative shift in angular orientation of the nodal diameters, the absolute location of the diameters is completely arbitrary.

0022-460X/00/090791 + 18 $35.00/0

Nominally axisymmetric structures with slight asymmetry due to, for example, inclusions or imperfections in the material or geometry or variations in boundary conditions lose their degeneracy characteristics and exhibit a phenomenon known as split modes [1–7]. The previously degenerate pair of modes now take on specific angular orientations that are independent of the spatial pattern of the excitation or initial conditions and dependent on the angular orientation of the asymmetry. The previously identical natural frequency values are now slightly shifted from one another, i.e., split. This is a well-known fact and has been studied in significant detail by a few researchers, particularly in regard to circular and annular plates [1–5]. Surprisingly, few focused studies of this behavior applied to cylindrical geometries can be found in the literature.

It is also surprising that few in-depth investigations can be found in the literature that describe using this phenomenon for non-destructive evaluation purposes. Critically important in the practical problem is the level of sensitivity in components which, of course, will never be perfectly axisymmetric even when no significant, localized flaw is present. In this paper, the use of "split-mode phenomena" coupled with a simple, inexpensive and rapid vibration measurement technique is investigated as a methodology for non-destructive evaluation. A basic theoretical motivation is offered and computational and experimental studies on cylindrical structures are reported. The level of specificity and sensitivity of the proposed NDE technique under practical confounding conditions, such as out-of-roundness, are investigated.

2. THEORY

Shen and Mote [2] formulated a perturbation method for the determination of the eigensolutions, Green's functions and steady state response of three-dimensional, finite, linear elastic solids containing small imperfections. Their focus was specifically on spectrally degenerate systems and explicit expressions were developed for circular plates with slot-like inclusions that disrupt the otherwise perfect axisymmetry. In this article, parts of their general formulation are explicitly applied to structures with ring-like geometry and small imperfections at specific angular locations. Without mathematical rigor, generalizations are then made to structures with cylindrical geometry and slot-like imperfections at particular axial positions and over specified angular ranges. Based in part on these findings a novel non-destructive technique for detecting localized imperfections, such as flaws in joints or cracks in cylindrical structures, is proposed.

Consider the circular ring shown in Figure 1 without any imperfections that destroy axisymmetry. Based on Soedel [8] we have the following for in-plane free vibrations of the axisymmetric circular ring:

$$L_1 u_\theta(\theta, t) - L_2 u_3(\theta, t) = 0, \quad L_2 u_\theta(\theta, t) - L_3 u_3(\theta, t) = 0, \tag{1a, b}$$

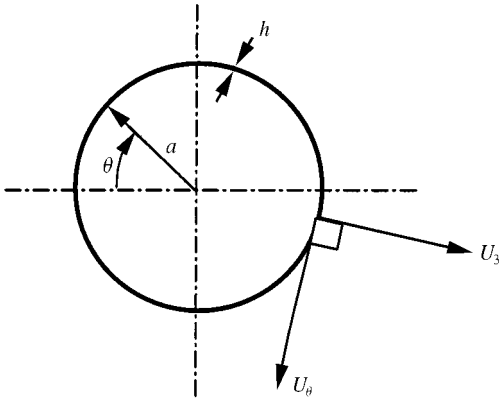

Figure 1. Axisymmetric circular ring.

where

$$L_1 = \frac{Eh}{a^2}\left[(1+p)\frac{\mathrm{d}^2}{\mathrm{d}\theta^2} - \frac{1}{\omega_0^2}\frac{\mathrm{d}^2}{\mathrm{d}t^2}\right], \quad L_2 = \frac{Eh}{a^2}\left[p\frac{\mathrm{d}^3}{\mathrm{d}\theta^3} - \frac{\mathrm{d}}{\mathrm{d}\theta}\right],$$

$$L_3 = \frac{Eh}{a^2}\left[1 + p\frac{\mathrm{d}^4}{\mathrm{d}\theta^4} + \frac{1}{\omega_0^2}\frac{\mathrm{d}^2}{\mathrm{d}t^2}\right], \quad \omega_0^2 = \frac{E}{\rho a^2}, \quad p = \frac{h^2}{12a^2}. \tag{1c–g}$$

Here, t, E, and ρ refer to time, the elastic modulus and the material density respectively. Refer to Figure 1 for definitions of the geometric variables.

The solution to the unperturbed problem can be obtained by setting $u_\theta(\theta,t) = U_\theta(\theta)\,\mathrm{e}^{\mathrm{j}\omega t}$ and $u_3(\theta,t) = U_3(\theta)\,\mathrm{e}^{\mathrm{j}\omega t}$. This leads to the following expressions for the eigenvalues ω_{n1}^2, ω_{n2}^2 (square of natural frequencies) and orthonormalized eigenfunctions Φ_{n1}, Φ_{n2}, Θ_{n1}, Θ_{n2} (normalized mode shapes with $U_{3nm}(\theta) \equiv \Phi_{nm}(\theta)$ and $U_{\theta nm}(\theta) \equiv (\Theta_{nm}(\theta))$.

$$\omega_{n1}^2 = \frac{K_1}{2}\left(1 - \sqrt{1 - 4K_2/K_1^2}\right), \quad \omega_{n2}^2 = \frac{K_2}{2}\left(1 + \sqrt{1 - 4K_2/K_1^2}\right), \quad n = 0, \pm 1, \pm 2, \cdots, \tag{2a, b}$$

$$\Phi_{nm}(\theta) = A_{nm}\cos(n[\theta + \alpha_{nm}]), \quad \Theta_{nm}(\theta) = A_{nm}\beta_{nm}\sin(n[\theta + \alpha_{nm}]),$$

$$n = 0, 1, 2, \cdots, m = 1, 2,$$

$$\Phi_{-nm}(\theta) = A_{-nm}\sin(n[\theta + \alpha_{-nm}]), \quad \Theta_{-nm}(\theta) = -A_{-nm}\beta_{-nm}\cos(n[\theta + \alpha_{-nm}]),$$

$$n = 1, 2, \cdots, m = 1, 2, \tag{2c–f}$$

where

$$K_1 = \frac{n^2+1}{a^2\rho h}\left(\frac{n^2 D}{a^2} + K\right), \quad K_2 = \frac{n^2(n^2-1)^2}{a^6(\rho h)^2}DK, \quad K = Eh, \quad D = Eh^3/12, \tag{2g–j}$$

$$A_{nm} = 1/\sqrt{\pi\rho h a(1+\beta_{nm}^2)}, \quad \beta_{nm} = \frac{(n/a^2)[n^2 D/a^2 + K]}{\rho h\omega_{nm}^2 - (n^2/a^2)[D/a^2 + K]}. \tag{2k, l}$$

In the above mode shape expressions, α_{nm} is completely arbitrary and $[\Phi_{nm}\ \Theta_{nm}]$ and $[\Phi_{-nm}\ \Theta_{-nm}]$ denote degenerate modes with identical natural frequency values for $n = 1, 2, \ldots$. In most ring applications, the case of $m = 1$ refers to a mode dominated by radial motion, U_3, and $m = 2$ refers to a mode dominated by circumferential motion, U_θ. Typically, $\omega_{n1} \ll \omega_{n2}$. Note that Φ_{01}, Θ_{01} with $\omega_{01} = 0$ denote a rigid-body mode where the ring is undeformed and spinning in plane about its axis. Likewise, $\Phi_{\pm 11}$, $\Theta_{\pm 11}$ with $\omega_{\pm 11} = 0$ denote rigid-body translation of the ring. The breathing mode of the ring is given by Φ_{02}, Θ_{02} with $\omega_{02} = \sqrt{K/a^2\rho h}$. Typically, none of these mentioned modes nor the remaining modes with $m = 2$ will involve significant bending motion of the ring. They, consequently, are not as much of interest to us as the $|n| \geqslant 2$, $m = 1$ modes in the intended NDE methodology. Nonetheless, the orthonormality conditions for all of the modes are as follows:

$$\int_0^{2\pi} \rho h a \{\Phi_{nm}(\theta)\,\Phi_{pq}(\theta) + \Theta_{nm}(\theta)\Theta_{pq}(\theta)\}\,\mathrm{d}\theta = \delta_{np}\delta_{mq}, \tag{3a, b}$$

$$\int_0^{2\pi} \left\{ \frac{Eh}{a} \begin{bmatrix} (1+p)\Theta''_{nm}(\theta) + p\Theta'''_{nm}(\theta) - p\Phi'''_{nm}(\theta) \\ +\Phi'_{nm}(\theta) - \Theta'_{nm}(\theta) - \Phi_{nm}(\theta) - p\Phi^{IV}_{nm}(\theta) \end{bmatrix} [\Theta_{pq}(\theta) + \Phi_{pq}(\theta)] \right\} \mathrm{d}\theta = \omega^2_{nm}\delta_{mp}\delta_{nq}.$$

Consider now that an imperfection centered at $\theta = \theta^e$ deg is present. The imperfection, which may be an inclusion or region of altered physical properties due to oxidation, delamination or some other aging-related phenomena is approximated by considering the impact that it has on the average property values in the region of the cross-section at θ^e deg. For example, if a slot is present which extends through a fraction δ of the axial width of the ring (not shown in Figure 1), then, at θ^e a modified set of physical properties, with subscript e, are specified: $E_e = (1 - \delta)E$ and $\rho_e = (1 - \delta)\rho$. The imperfection will also extend in the θ direction by some value ε radians.

Following the methodology of Shen and Mote [2] as detailed in their Appendix B for the general problem, approximations for natural frequencies and mode shapes for the ring with the imperfection can be obtained as perturbations from those of the ideal axisymmetric case. If there is one imperfection at $\theta_e = 0$ then $\alpha_{nm} = 0$. In other words, the angle of the slightly non-degenerate eigenfunctions is not arbitrary as it is for the corresponding unperturbed, degenerate eigenfunctions. Application of the perturbation theory leads to the following expressions for calculation of the split modes associated with predominantly radial motion $\Psi_{n1}(\theta)$ and $\Psi_{-n1}(\theta)$, and their associated natural frequencies v_{n1} and v_{-n1}. Note that a second order perturbation is employed for calculation of the natural frequencies as the first order perturbation is negligible:

$$\Psi_{n1}(\theta) \approx \Phi_{n1}(\theta) + \sum_{\substack{p=-\infty \\ |p| \neq |n|}}^{\infty} \frac{d^{p1}_{n1}}{\omega^2_{n1} - \omega^2_{p1}} \Phi_{p1}(\theta) + O(\varepsilon^2) \tag{4a}$$

and

$$v^2_{n1} \approx \omega^2_{n1} + \overset{0}{\overset{\uparrow}{d}}{}^{n1}_{n1} + \sum_{\substack{p=-\infty \\ |p| \neq |n|}}^{\infty} \frac{d^{p1}_{n1} d^{n1}_{p1}}{[\omega^2_{n1} - \omega^2_{p1}]} + O(\varepsilon^3), \tag{4b}$$

TABLE 1

Aluminum cylinder example case parameter values

$E = 73 \times 10^9$ N/m^2
$\rho = 2700$ kg/m^3
$v = 0{\cdot}33$
$a = 49{\cdot}1744$ mm
$h = 3{\cdot}2512$ mm
$L = 381{\cdot}0$ mm

where

$$d_{rs}^{pq} = \omega_{nm}^2 \langle \mathbf{U}_{rs} | \mathbf{U}_{pq} \rangle_{\rho 1} - \langle \mathbf{U}_{rs} | \mathbf{U}_{pq} \rangle_{E1} = O(\varepsilon), \tag{4c}$$

$$\langle \mathbf{U}_{rs} | \mathbf{U}_{pq} \rangle_{\rho 1} = \int_{\theta^e - \varepsilon/2}^{\theta^e + \varepsilon/2} \rho_1 ha \{ \Phi_{rs}(\theta)\, \Phi_{pq}(\theta) + \Theta_{rs}(\theta) \Theta_{pq}(\theta) \}\, \mathrm{d}\theta$$

$$\approx \varepsilon \rho_1 ha \{ \Phi_{rs}(0)\, \Phi_{pq}(0) + \Theta_{rs}(0) \Theta_{pq}(0) \} = O(\varepsilon), \tag{4d}$$

$$\langle \mathbf{U}_{rs} | \mathbf{U}_{pq} \rangle_{E1} = \int_{\theta^e - \varepsilon/2}^{\theta^e + \varepsilon/2} \left\{ \frac{E_1 h}{a} \begin{bmatrix} (1+p)\Theta_{rs}''(\theta) + p\Theta_{rs}'''(\theta) - p\Theta_{rs}'''(\theta) \\ + \Phi_{rs}'(\theta) - \Theta_{rs}'(\theta) - \Phi_{rs}(\theta) - p\Phi_{rs}^{IV}(\theta) \end{bmatrix} \right.$$

$$\left. \times [\Theta_{pq}(\theta) + \Phi_{pq}(\theta)] \right\} \mathrm{d}\theta,$$

$$\approx \frac{\varepsilon E_1 h}{a} \begin{bmatrix} (1+p)\Theta_{rs}''(0) + p\Theta_{rs}'''(0) - p\Phi_{rs}'''(0) \\ + \Phi_{rs}'(0) - \Theta_{rs}'(0) - \Phi_{rs}(0) - p\Phi_{rs}^{IV}(0) \end{bmatrix}$$

$$\times [\Theta_{pq}(0) + \Phi_{pq}(0)] = O(\varepsilon). \tag{4e}$$

Consider the unrestrained "ring" with dimensions given in Table 1 and shown in Figure 2. Consider the cases of perfect axisymmetry and that of a slot present with dimensions $\delta = 5$ mm centered at the mid-point of the axial length and $\varepsilon = 10$ or 30° centered at $\theta_e = 0^\circ$. This geometry would more aptly be specified as a cylinder under free end conditions with the following unperturbed mode shape expressions for predominantly radial vibratory motion replacing those of equations (2c, e) [9]:

$$\Phi_{n1q}(\theta, x) = A_{n1q} \cos(n[\theta + \alpha_{nm}]) Q_q(x), \quad n = 0, 1, 2, \ldots, \quad q = 0, 1, 2, \ldots,$$

$$\Phi_{-n1q}(\theta, x) = A_{-n1q} \sin(n[\theta + \alpha_{-nm}]) Q_q(x), \quad n = 1, 2, \ldots, \quad q = 0, 1, 2, \ldots. \tag{5a, b}$$

The axial function $Q_q(x)$ can be described in terms of the number q of nodal circumferences, axial locations with zero transverse motion for all values of θ. For each pair of degenerate modes Φ_{n1q} there will be a natural frequency ω_{n1q}. For

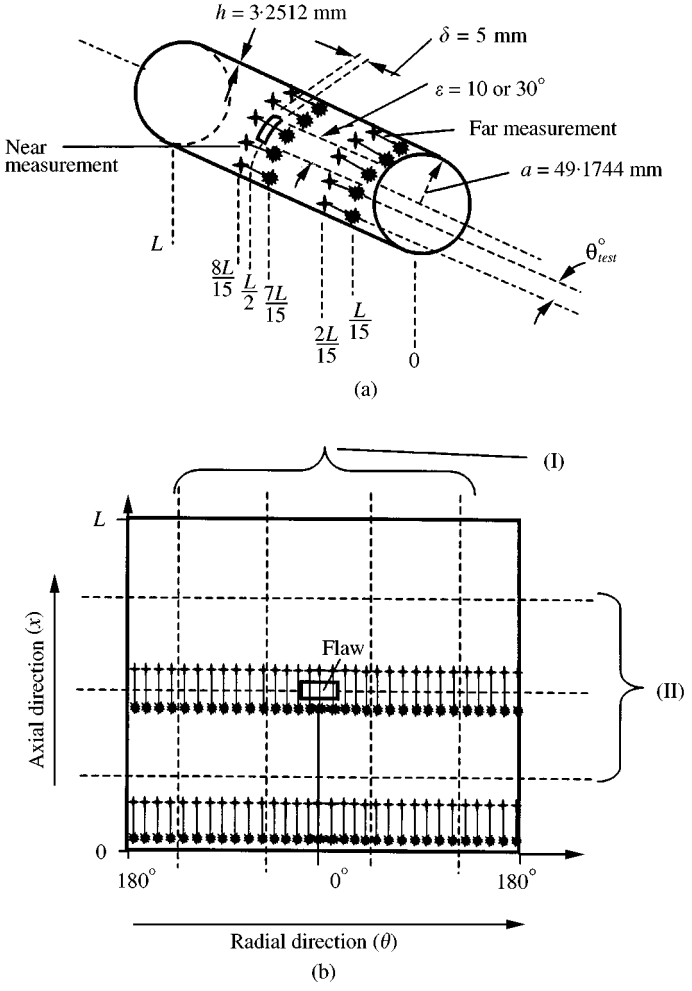

Figure 2. Schematic of the test structure and excitation points for "nearly degenerate" NDE technique. (a) Cylindrical test structure, (b) unwrapped cylindrical shell denoting modal index naming convention. ∗, impact point; +, corresponding measurement point. The line connects the corresponding impact/measurement pairs. There were 36 simulated impact/measurement pairs separated circumferentially by $\theta_{test} = 10^\circ$ using ANSYS at both "near" and "far" measurement locations (Figures 5–10). There were 32 experimental impact/measurement pairs separated circumferentially by $\theta_{test} = 11{\cdot}25^\circ$ at both "near" and "far" measurement locations (Figures 11 and 12). (I) Even number of node lines in radial direction. Mode index is half this ($n = 2$). (II) Node lines in axial direction = mode index in axial direction ($q = 3$).

ring-like motion with no nodal circumferences, we have $q = 0$. If there are nodal circumferences, q specifies the number of nodal circumferences as in Figure 2.

The developed perturbation theory for ring geometry can be used to predict the perturbed natural frequencies and mode shapes for the $q = 0$ axial order modes. In Table 2, theoretical predictions are given for the unperturbed (equation (2a)) and perturbed (equation (4b)) natural frequencies under specified slot conditions and with the cylindrical geometry and material properties given in Table 1. Note that the modulus of elasticity E is replaced by $E/(1 - \nu^2)$ in the above formulations

TABLE 2

Theoretical predictions of natural frequencies $\nu_{n10}/2\pi$ *(Hz) for case of* $q = 0$ *axial modal order*

Circumferential order	No slot: $\varepsilon = 0$ $\delta = 0$	Slot: $\varepsilon = 10^\circ$ $\delta = 5/381$ $= 0{\cdot}013$	Slot: $\varepsilon = 30^\circ$ $\delta = 5/381$ $= 0{\cdot}013$
$n = 2$	912·6	913·1/914·2	914·2/919·1
$n = 3$	2581	2582/2588	2583/2602
$n = 4$	4948	4949/4962	4951/4990

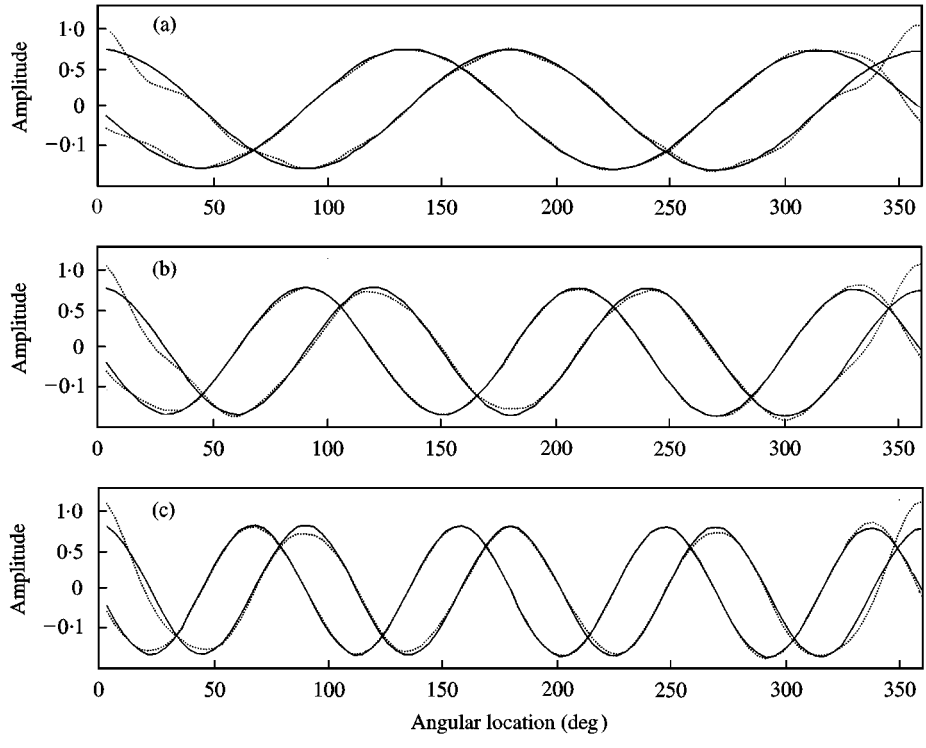

Figure 3. Theoretical results. Normalized unperturbed and perturbed mode shapes corresponding to natural frequency values listed in Table 2 for a slot of angular length $\varepsilon = 30^\circ$. (a) $n = \pm 2$, $p = 0$ modes, (b) $n = \pm 3$, $p = 0$ modes, (c) $n = \pm 4$, $p = 0$ modes: ——, unperturbed mode shapes; ---, perturbed mode shapes.

where ν is the Poisson ratio. This is done to approximate a plane strain condition in the axial "x" direction of the cylinder that should be more realistic. Theoretical predictions of the corresponding unperturbed (equation (2c, e)) and perturbed (equation (4a)) mode shapes are shown in Figure 3.

Explicit mathematical predictions for the perturbed eigensolutions for the other $q \neq 0$ modes could be developed but are beyond the scope of this article. One would

expect that these nominally degenerate modes would be split in a similar fashion to the $q = 0$ modes. The slot's proximity axially with respect to axial nodal circumferences of unperturbed solutions may affect the strength of the perturbation for a particular $q \neq 0$ solution. Also, similar to the decay in the strength of the perturbation of the mode shape as one moves away circumferentially from the localized flaw (slot), one would expect an additional decay in the strength of the perturbation of the mode shape as one moves away from it axially.

3. A "NEARLY DEGENERATE" NDE TECHNIQUE

Consider now that the test structure is driven with an impact excitation at a range of different angular locations around the circumference of the circular object at a particular axial location as shown in Figure 2. The theory suggests that the two nearly degenerate modes will be excited at relatively different levels depending on the angular location. If one measures the response at the same circumferential (θ) position as the impact, the more strongly excited nearly degenerate mode will be more directly measured. A non-contacting laser Doppler vibrometer (LDV) could be reflected perpendicular to the shell surface near the point of impact to record the response of the structure. Use of the non-contacting sensor avoids mass loading of the structure and the introduction of additional non-axisymmetry. Alternatively, a successful measurement might be made with a closely placed, less-expensive microphone. In theory, the described approach ought to lead to the detection and location of a flaw in an otherwise nominally axisymmetric cylindrical structure.

The practical issue, of course, is the level of sensitivity that can be attained given that (a) no structure is truly axisymmetric to begin with, and (b) there are limitations on the level of frequency resolution that can be achieved for a given data acquisition system. The capabilities and limitations of the proposed technique were explored for the cylindrical geometry given in Table 1 via numerical and experimental studies that are summarized in the following sections.

4. FINITE ELEMENT STUDIES

To test the above theoretical formulations and investigate the proposed "nearly degenerate" NDE strategy, the technique was simulated using ANSYS Version 5.4 Finite Element software with the geometric and material properties provided in Table 1. The ANSYS model is shown in Figure 4 and is composed of eight-node "Shell93" elements. It was precisely constructed using the direct generation technique, not an automated mesh generation procedure, in order to avoid introducing unintended non-axisymmetry. The "frequency response" solution routine in ANSYS was utilized to simulate the novel NDE technique. Unit radial point forces were applied at specified locations and the radial motion response recorded at corresponding locations per Figure 2. ANSYS solution routine choices had to be made carefully to avoid the introduction of non-axisymmetry numerically. The mode superposition approach was taken as opposed to the full or

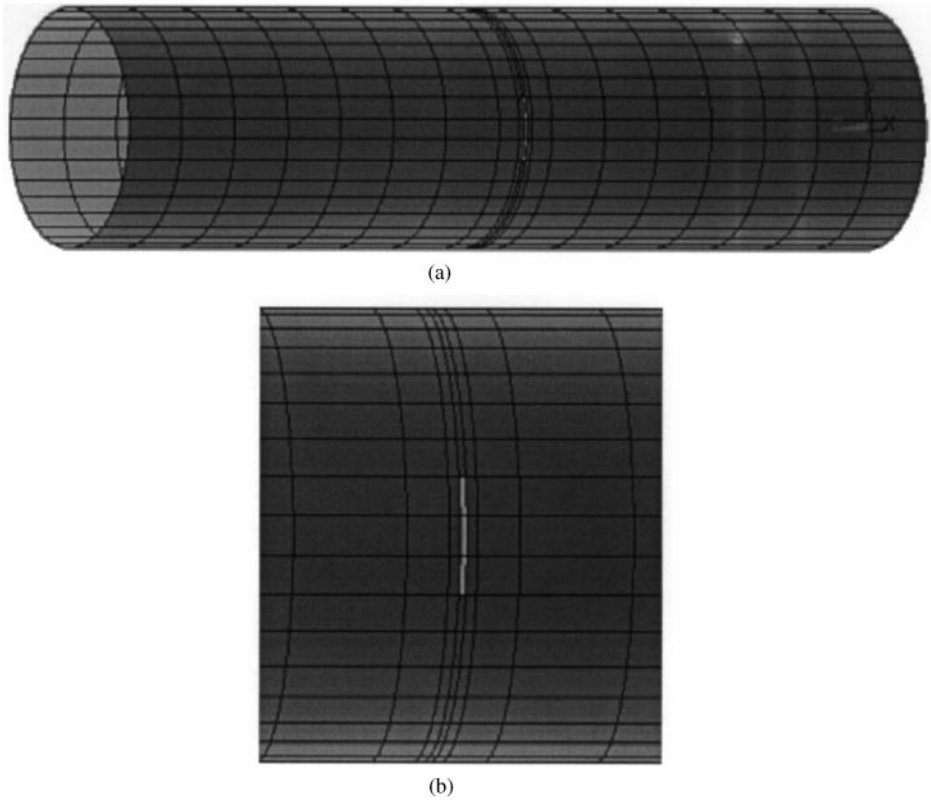

Figure 4. ANSYS finite element model (FEM) of the test structure that is depicted in Figure 2: (a) entire structure, (b) close-up of slot region.

reduced method that requires specification of master degrees of freedom. It was found that these methods introduced numerical non-axisymmetries to the problem whereas the mode superposition method does not, at least to machine precision. Also, it was necessary to remove the six rigid-body modes before running the analysis routine by using the "rigid,all" command in ANSYS.

Finite element natural frequency predictions are provided in Table 3 for the axisymmetric baseline case and two cases with specified slot dimensions identical to the cases described in section 2. For the $q = 0$ modes, direct comparison with the theoretical predictions provided in Table 2 show agreement in important trends, although quantitative discrepancies exist. Certainly, a more refined mesh with more uniform element geometric aspect ratios may have yielded more accurate results. But, the current model captures the salient feature, namely the splitting of natural frequency pairs and the alteration of mode shapes.

Results of the FEM simulation of the "nearly degenerate" NDE technique for various cases are shown in Figures 5–10. In each figure, the response for two pairs of nominally degenerate or nearly degenerate modes are highlighted, the cases of $n = \pm 2$, $q = 0$ and $n = \pm 2$, $q = 2$. The figures show, as a function of circumferential excitation location θ and axial location ("near" or "far" in

TABLE 3

FEM predictions of natural frequencies $v_{n1q}/2\pi$ *(Hz)*

Circumferential (n) and axial order	No slot: $\varepsilon = 0$ $\delta = 0$	Slot: $\varepsilon = 10^\circ$ $\delta = 5/381$ $= 0{\cdot}013$	Slot: $\varepsilon = 30^\circ$ $\delta = 5/381$ $= 0{\cdot}013$
$\boldsymbol{n = 2, q = 0}$	**907·6**	**907·4/907·6**	**907·2/907·6**
$n = 2, q = 1$	927·8	927·8/927·8	927·7/927·8
$n = 2, q = 2$	1656	1653·0/1656·0	1629·5/1655·3
$\boldsymbol{n = 3, q = 0}$	**2553**	**2552·2/2552·5**	**2551·7/2552·4**
$n = 3, q = 1$	2574	2574·1/2574·1	2574·1/2574·1
$n = 3, q = 2$	2771	2769·6/2770·8	2763·6/2770·2
$n = 1, q = 2$	3297	3289·6/3297·1	3230·6/3297·1
$n = 3, q = 3$	3350	3350·0/3350·0	3348·8/3349·9
$n = 2, q = 3$	3351	3348·1/3350·5	3333·0/3350·2
$n = 3, q = 4$	4361	4356·8/4360·8	4330·3/4358·6
$\boldsymbol{n = 4, q = 0}$	**4851**	**4850·6/4850·8**	**4850·3/4850·7**
$n = 4, q = 1$	4865	4864·7/4864·7	4864·7/4864·7

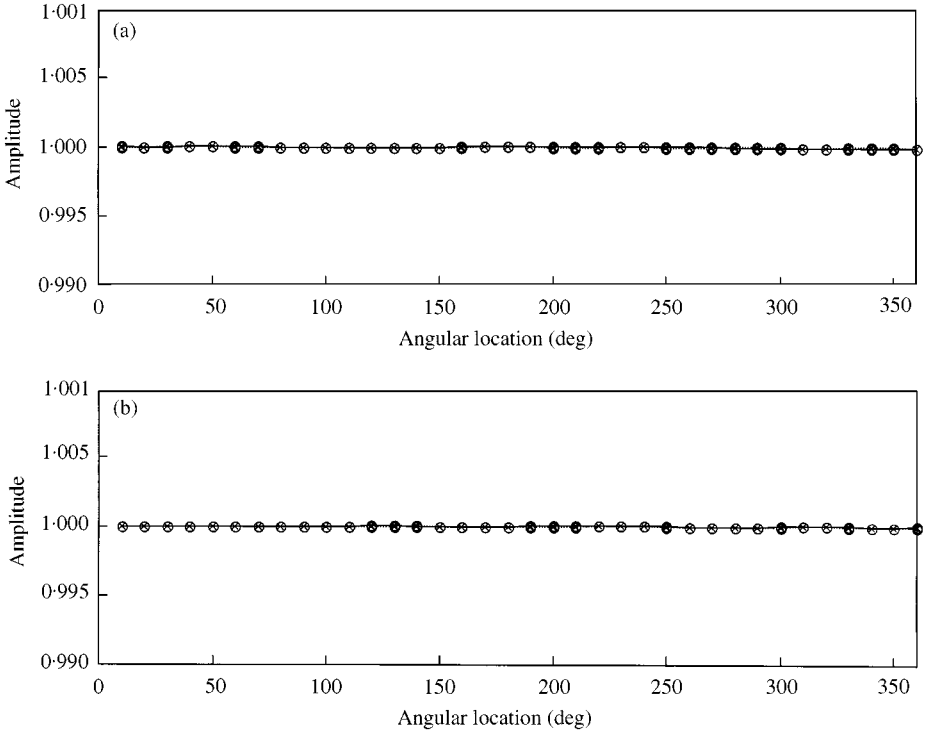

Figure 5. FEM results. "Near" and "far" application of NDE technique as in Figure 2. For this case, no slot is present and the structure has perfect axisymmetry. Normalized frequency response magnitude at selected resonant frequencies is shown as a function of angular excitation/measurement position. (a) $n = \pm 2$, $p = 0$ modes, (b) $n = \pm 2$, $p = 2$ modes: ——, near measurement; ----, far measurement; × × ×, ○○○, 907·6/1656 Hz.

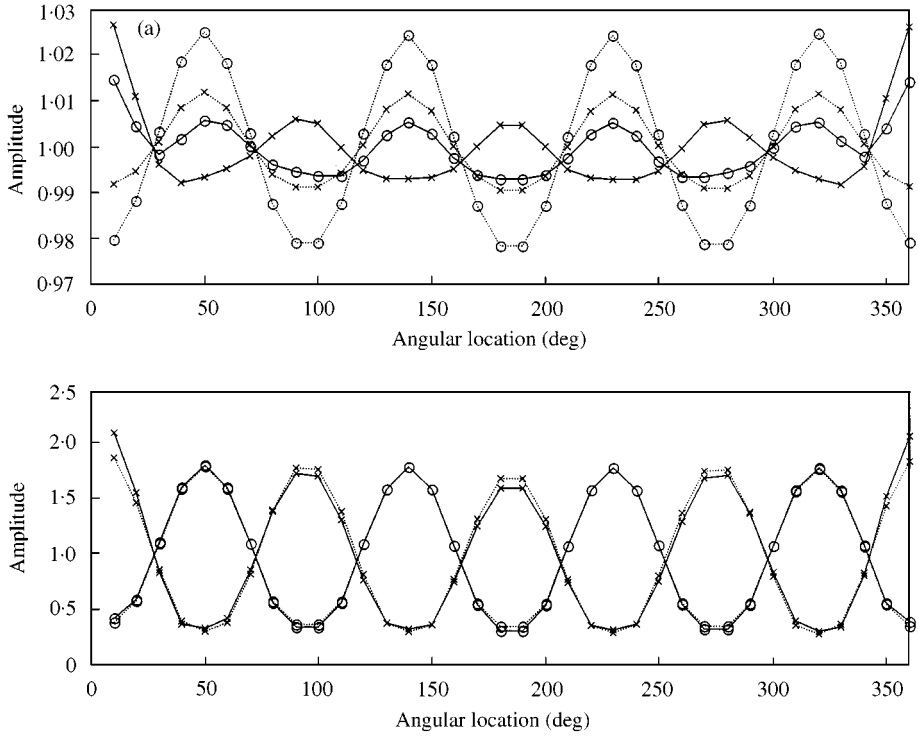

Figure 6. FEM results. Application of NDE technique as in Figure 2. For this case, slot dimensions are 5 mm axially and 30° circumferentially. Normalized frequency response magnitude at selected resonant frequencies is shown as a function of angular excitation/measurement position. (a) $n = \pm 2$, $p = 0$ modes, (b) $n = \pm 2$, $p = 2$ modes: ——, near measurement; ----, far measurement, × × ×, 907·2/1629 Hz; ○○○, 907·6/1655 Hz.

Figure 2), the normalized magnitude of the frequency response for a given excitation/measurement pair in Figure 2. Normalization (and non-dimensionalization) is achieved by dividing the magnitude of the response for a particular excitation/measurement pair by the average magnitude of the response for the entire set of 36 (10° increments) excitation/measurement pairs made at the corresponding "near" or "far" axial location. In other words, a measurement made at the far axial location is divided by the average of all 36 measurements made at the far axial location.

For the baseline case shown in Figure 5, as expected no variation is seen in the magnitude of the response as a function of θ for either mode at either "near" or "far" locations. For the case of a $\varepsilon = 30°$ slot shown in Figure 6, clearly non-axisymmetry exists and the dominant mode of the split mode pair alternates as a function of θ. Also note that in the circumferential vicinity of the slot, a localized anomaly in the pattern exists, with an increase in the magnitude of the response. Hence, not only is the existence of the "flaw" predicted, but its circumferential location is also pinpointed. Comparison between "near" and "far" measurement sets, particularly for mode $n = \pm 2, q = 2$ (Figure 6(b)), hints at the axial position of the "flaw" as the magnitude of the anomaly is greater at the nearer location. These observed

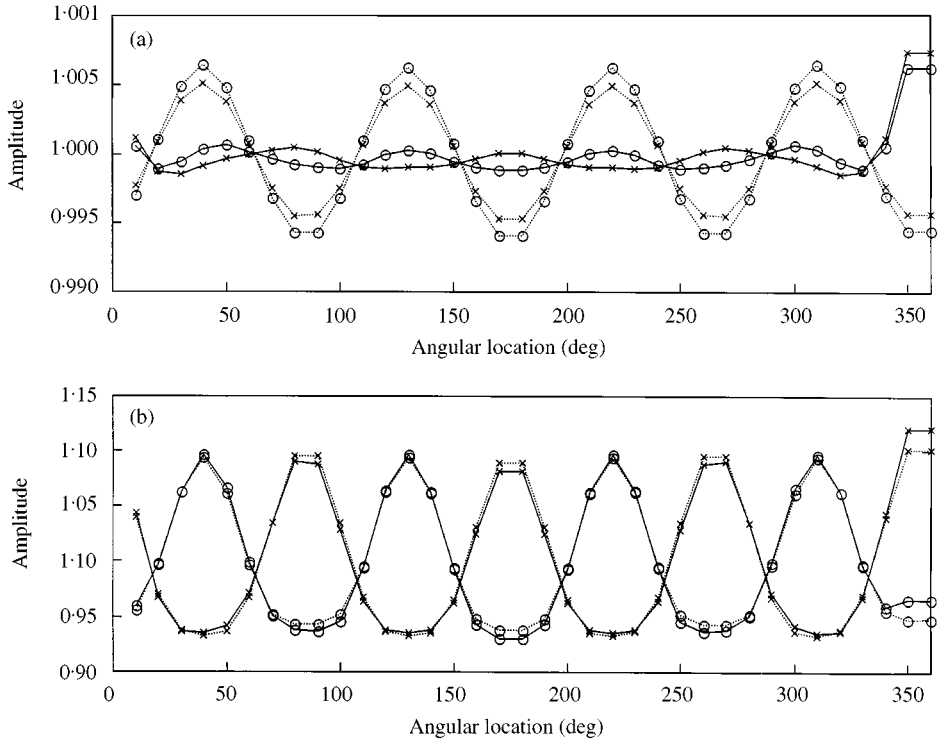

Figure 7. FEM results. Application of NDE technique as in Figure 2. For this case, slot dimensions are 5 mm axially and 10° circumferentially. Normalized frequency response magnitude at selected resonant frequencies is shown as a function of angular excitation/ measurement position. (a) $n = \pm 2$, $p = 0$ modes, (b) $n = \pm 2$, $p = 2$ modes: ——, near measurement; ----, far measurement; × × ×, 907·5/1653 Hz; ○○○, 907·6/1656 Hz.

tendencies agree with the theoretical predictions of section 2. Identification of these tendencies is not as straightforward for the $n = \pm 2$, $q = 0$ modes (Figure 6(a)) because of another effect.

In the ANSYS model, modal damping values of 0·5% of critical damping were specified for each mode in the mode superposition solution approach. Split natural frequencies for $n = \pm 2$, $q = 0$ do not result in split resonant peaks in the frequency response prediction due to the level of damping combined with their close proximity. Hence, particularly for the far measurement case where the effect of the anomaly is reduced, it appears that the response at the natural frequency of the $n = -2$ "x" mode is dominated by the response at the natural frequency of the $n = +2$ "o" mode. Nonetheless, it is clear from the figure, that the circumferential location of the "flaw" is evident as well as the axial location, given the increase in strength of anomalies in the magnitude value. In Figure 7, the response for an $\varepsilon = 10°$ slot is shown. Here, trends similar to those depicted in Figure 6 for $\varepsilon = 30°$ are evident but with reduced strength, indicating a limitation to the NDE technique's sensitivity.

One would expect that eccentricity or "out-of-roundness" of the cylinder would also result in similar split mode behavior and fluctuations in the magnitude of

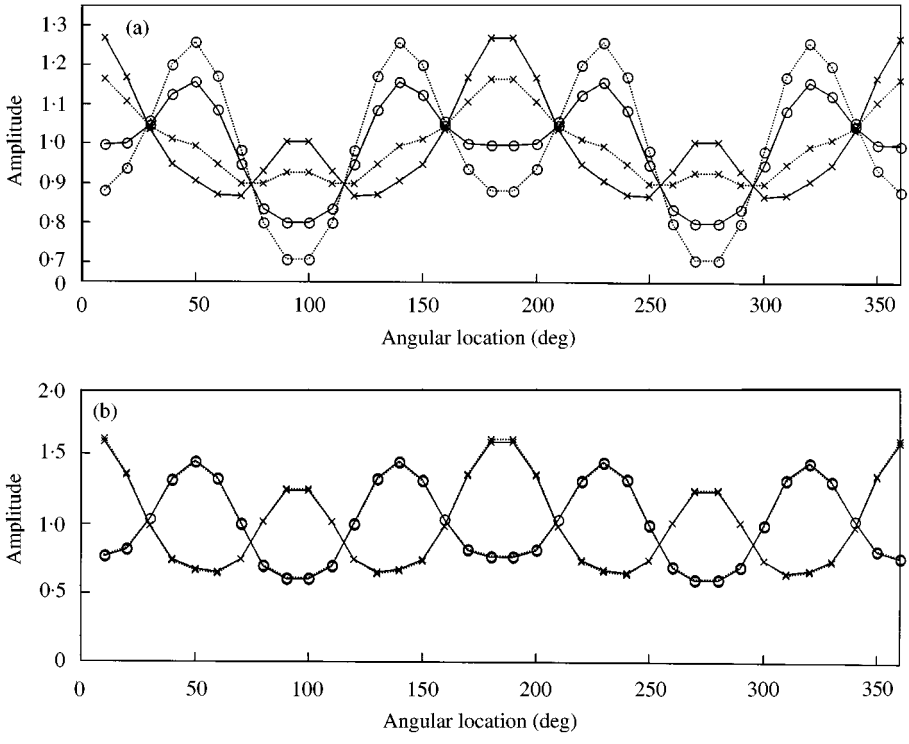

Figure 8. FEM results. Application of NDE technique as in Figure 2. For this case, no localized slot is present but an out-of-round condition exists of eccentricity $e = 0{\cdot}05$. Normalized frequency response magnitude at selected resonant frequencies is shown as a function of angular excitation/measurement position. (a) $n = \pm 2$, $p = 0$ modes, (b) $n = \pm 2$, $p = 2$ modes: ——, near measurement; ----, far measurement; × × ×, 899·9/1644 Hz; ○○○, 902·0/1653 Hz.

response for the NDE technique. Since no actual cylindrical structure can be fabricated with perfect axisymmetry a practical issue is whether or not one can distinguish between the effect of eccentricity and that of a localized flaw, such as a slot or crack, using the proposed NDE technique. This was investigated by using ANSYS to simulate application of the NDE technique to a cylinder with eccentricity in geometry of $e = 0{\cdot}05$ as specified by the following equation for the radius a as a function of θ (rad):

$$a = 49{\cdot}1744/(1 + 0{\cdot}05\cos(2\theta))\ \text{mm}. \tag{6}$$

Results of the FEM simulation for the eccentric case described by equation (6) are shown in Figure 8. As hypothesized, the eccentric condition does result in split-mode behavior and a periodic fluctuation in the magnitude of the response as a function of θ. However, there is not a localized anomaly in the fluctuation pattern as was the case when a localized flaw was present. Hence, the cases can be distinguished. Results of the simulation of the case where both eccentricity and the flaw are present are shown in Figures 9 and 10 for the same eccentricity $e = 0{\cdot}05$ and two slot dimensions, $\varepsilon = 10$ and 30°. Here, it is observed that, while anomalies

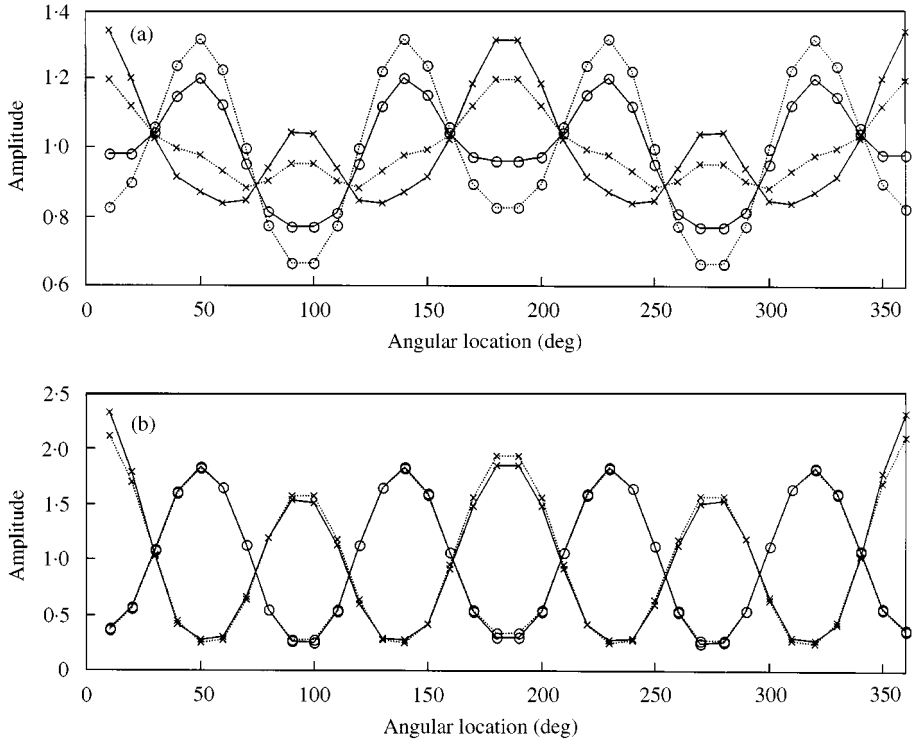

Figure 9. FEM results. Application of NDE technique as in Figure 2. For this case, slot dimensions are 5 mm axially and 30° circumferentially and out-of-round condition exists with eccentricity $e = 0{\cdot}05$. Normalized frequency response magnitude at selected resonant frequencies is shown as a function of angular excitation/measurement position. (a) $n = \pm 2$, $p = 0$ modes, (b) $n = \pm 2$, $p = 2$ modes: ——, near measurement; ----, far measurement; × × ×, 899·5/1621 Hz; ○○○, 902·1/1653 Hz.

in the fluctuation pattern exist that are indicative of a localize flaw, they are slightly less obvious than they were with zero eccentricity.

5. EXPERIMENTAL STUDIES

Next, the proposed NDE technique was tested experimentally using sections of an aluminum tube that was fabricated by extrusion. A baseline case and the case of the 30° slot used for the FEM and theoretical studies were tested. Thirty-two equally spaced measurements were made around the circumference at near and far locations as in Figure 2 using an impulse hammer (PCB Model #086B01) for excitation and a Laser Doppler Vibrometer (Polytec PI Model CLV-700/800) for measurement. The vibrometer head was placed at its optimal focal length of 315 mm from the tube surface with the beam impinging perpendicular to the surface to measure radial surface velocity. Transducer signals were captured and the frequency response functions calculated using the Hewlett Packard 35670 two-channel dynamic signal analyzer. Also, experimental modal analysis was performed using a grid of 128 points (16 circumferential and 8 axial) and STAR

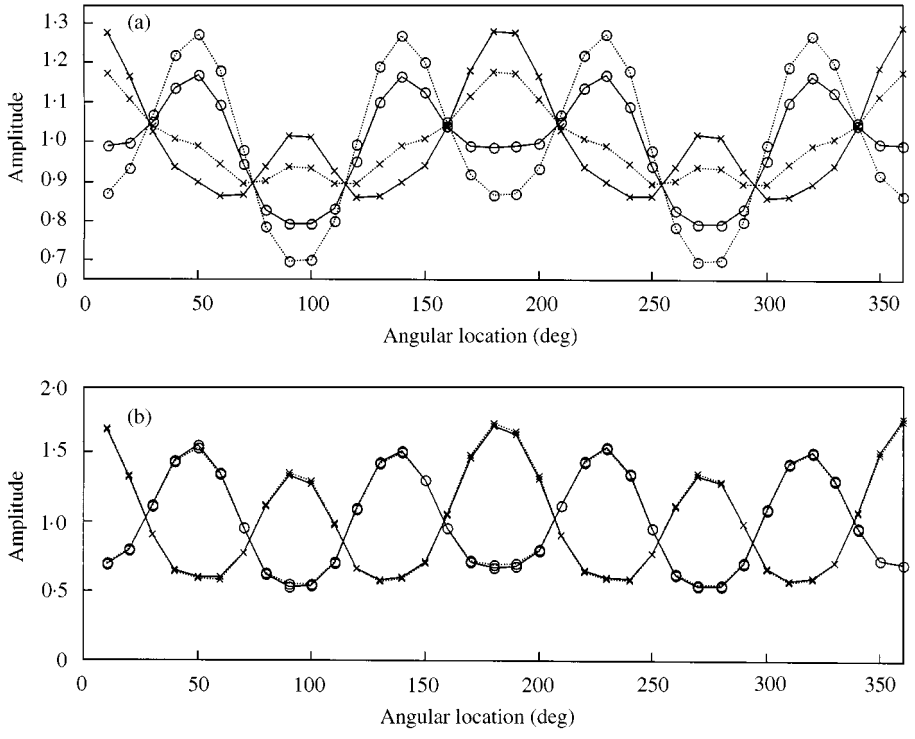

Figure 10. FEM results. Application of NDE technique as in Figure 2. For this case, slot dimensions are 5 mm axially and 10° circumferentially and out-of-round condition exists with eccentricity $e = 0{\cdot}05$. Normalized frequency response magnitude at selected resonant frequencies is shown as a function of angular excitation/measurement position. (a) $n = \pm 2$, $p = 0$ modes; (b) $n = \pm 2$, $p = 2$ modes: ——, near measurement; ----, far measurement; × × ×, 899·8/1641 Hz; ○○○, 902·1/1653 Hz.

Modal software resident on a PC and controlling the Hewlett Packard 35670 to confirm which modes were associated with which resonant peaks. Natural frequency estimates as a function of modal indices are given in Table 4. Comparison with FEM results in Table 3 and theoretical values in Table 2 qualitatively confirm the split mode trends although quantitative discrepancies do exist.

Results of the experimental application of the "nearly degenerate" NDE technique for the various cases are shown in Figures 11 and 12. The selected results and method for graphical display are analogous to those of the FEM simulation depicted in Figures 5 and 6. For the baseline case shown in Figure 11, minimal but non-negligible variation is observed in the magnitude of the response as a function of θ for either mode at either "near" or "far" locations. For the case of an $\varepsilon = 30°$ slot shown in Figure 12, non-axisymmetry exists and the dominant mode of the split mode pair alternates as a function of θ. A localized anomaly in the fluctuating pattern does indeed exist, indicative of the localized flaw. It is not as obvious as that depicted in the FEM simulation due to the presence of anomalous behavior already present in the baseline case. The impact of frequency resolution in the application of the NDE technique was also investigated with results highlighted in Figure 12.

TABLE 4

Experimental measurements of natural frequencies $v_{n1q}/2\pi$ (Hz) using modal analysis

Circumferential (n) and axil (q) order	No slot: $\varepsilon = 0$ $\delta = 0$ (Hz)	Slot: $\varepsilon = 30^\circ$ $\delta = 5/381$ mm $= 0{\cdot}013$ (Hz)
$\boldsymbol{n = 2, q = 0}$	**916**	**916·3/919·0**
$n = 2, q = 1$	940	939·8/939·8
$n = 2, q = 2$	1644	1614/1640
$\boldsymbol{n = 3, q = 0}$	**2580**	**2583/2590**
$n = 3, q = 1$	2610	2605/2609
$n = 3, q = 2$	2800	2797/2804
$n = 1, q = 2$	3250	3173/3273
$n = 3, q = 3$	3370	3361/3363
$n = 2, q = 3$	3300	3279/3292
$n = 3, q = 4$	4360	4328/4356
$\boldsymbol{n = 4, q = 0}$	**4920**	**4918/4927**
$n = 4, q = 1$	4950	4929/4952

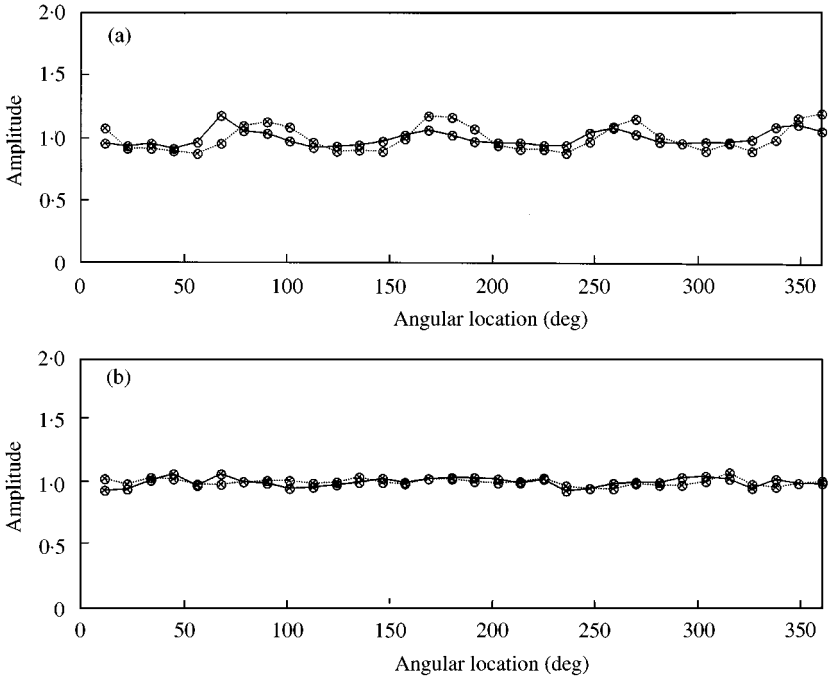

Figure 11. Experimental measurements. Application of NDE technique as in Figure 2. For this case, no slot is present. Normalized frequency response magnitude at selected resonant frequencies is shown as a function of angular excitation/measurement position. (a) $n = \pm 2, p = 0$ modes, (b) $n = \pm 2$, $p = 2$ modes: ——, near measurement; ----, far measurement; × × ×, ○○○, 916/1644 Hz.

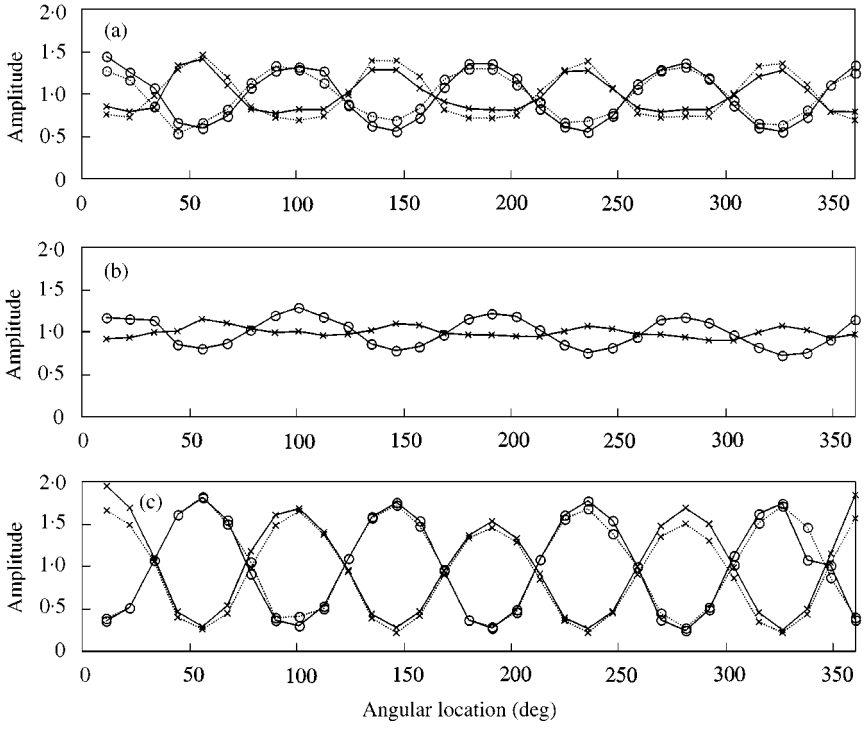

Figure 12. Experimental measurements. Application of NDE technique as in Figure 2. For this case, slot dimensions are 5 mm axially and 30° circumferentially. Normalized frequency response magnitude at selected resonant frequencies is shown as a function of angular excitation/measurement position. (a) $n = \pm 2$, $p = 0$ modes, frequency resolution = 1 Hz. (b) $n = \pm 2$, $p = 0$ modes, frequency resolution = 4 Hz: (c) $n = \pm 2$, $p = 2$ modes, frequency resolution = 4 Hz;. ——, near measurement; ----, far measurement; × × ×, 916/1614 Hz; ○○○, 919(920)/1640 Hz.

Improved frequency resolution yields greater fluctuations in the magnitude levels of the frequency response as a function of angular position. This results in greater sensitivity of the NDE technique.

6. CONCLUSIONS

Theoretical motivation and computational and experimental verification studies have been reported on a novel technique utilizing split-mode phenomena in nominally axisymmetric structures for the non-destructive detection of localized inclusions, such as joint flaws. Results of the analytical, computational and experimental studies verify the basic premises behind the proposed NDE methodology and provide an assessment of the level of specificity and sensitivity of the technique under practical confounding conditions, such as out-of-roundness.

There are a number of issues that merit further investigation. Theoretically, an explicit derivation of the perturbation theory for cylindrical geometries would be helpful. Also, the effect of confounding conditions that contribute to

non-axisymmetry but are not considered flaws should be further explored. For example, the impact of asymmetric boundary conditions on the cylindrical structure was not addressed. Arguably, as a practical solution to this problem, one might effectively "clamp-off" a length of the cylinder for testing. The clamps could provide the needed axisymmetric boundary conditions. Note also that flanges at the end of a pipe or cylindrical section often do effectively isolate it, behaving like simply supported boundary conditions for $n \geqslant 2$ circumferential modes [9]. The effect of multiple localized flaws should also be investigated. Additionally, use of a less expensive microphone or other non-contacting sensors in place of the laser Doppler vibrometer should be explored. Finally, the investigation could be expanded to other nominally axisymmetric structures and geometries.

ACKNOWLEDGMENT

Partial support for this work from the U.S. Department of Energy, Office of Basic Energy Sciences, Materials: center of excellence for synthesis and processing of advanced materials is acknowledged. Mr Sung-Han Kim is acknowledged for his assistance in conducting the experimental work.

REFERENCES

1. R. C. Yu and C. D. Mote Jr 1987 *Journal of Sound and Vibration* **119**, 409–427. Vibration and parametric excitation in asymmetric circular plates under moving loads.
2. I. Y. Shen and C. D. Mote Jr 1992 *Journal of Sound and Vibration* **155**, 443–465. Dynamic analysis of finite linear elastic solids containing small elastic imperfections: theory with application to asymmetric circular plates.
3. H. Vinayak and R. Singh 1996 *Journal of Sound and Vibration* **192**, 741–769. Eigensolutions of annular-like elastic disks with intentionally removed or added material.
4. R. G. Parker and C. D. Mote Jr 1996 *Journal of Vibration and Acoustics* **118**, 436–445. Exact perturbation for the vibration of almost annular or circular plates.
5. R. G. Parker and C. D. Mote Jr 1998 *Journal of Sound and Vibration* **211**, 389–407. Exact boundary condition perturbation for eigensolutions of the wave equation.
6. A. W. Leissa 1969 *Vibration of Plates*, *NASA SP*-160. Washington, DC.: U.S. Government Printing Office.
7. A. W. Leissa 1973 *Vibration of Shells*, *NASA SP*-288. Washington, DC.: U.S. Government Printing Office.
8. W. Soedel 1993 *Vibrations of Shells and Plates*: *revised and Expanded*. New York: Marcel Dekker, Inc. Second edition.
9. T. J. Royston 1995 *The Noise Control Engineering Journal* **43**, 15–20. Shaped PVDF sensors for intelligent measurement of plane wave acoustic pressure in liquid-filled pipes.